Journal of The Korean Astronomical Society
40: 1 ∼ 7, 2007

POLARIZATION OF THOMSON SCATTERED LINE RADIATION FROM BROAD ABSORPTION LINE OUTFLOWS IN QUASARS

Kyoung Min Baek[1], Jeong Hoon Bang[1], Yeon-Kyeong Jeon[1], Suna Kang[2], and Hee-Won Lee[2]
[1] Uijeongbu Science High School, Korea
E-mail: tnback@hanmail.net, banggl89@naver.com, 0dusrud0@naver.com
[2] Department of Astronomy and Space Science, Sejong University, Seoul 143-747, Korea
E-mail: sunakang@arcsec.sejong.ac.kr, hwlee@sejong.ac.kr
(Received February 6, 2007; Accepted February 16, 2007)

ABSTRACT

About 10 percent of quasars are known to exhibit deep broad absorption troughs blueward of prominent permitted emission lines, which are usually attributed to the existence of outflows slightly above the accretion disk around the supermassive black hole. Typical widths up to $0.2c$ of these absorption troughs indicate the velocity scales in which special relativistic effects may not be negligible. Under the assumption of the ubiquity of the broad absorption line region in quasars, the broad emission line flux will exhibit Thomson scattered components from these fast outflows. In this paper, we provide our Monte Carlo calculation of linear polarization of singly Thomson scattered line radiation with the careful considerations of special relativistic effects. The scattering region is approximated by a collection of rings that are moving outward with speeds $v = c\beta < 0.2c$ near the equatorial plane, and the scattered line photons are collected according to its direction and wavelength in the observer's rest frame. We find that the significantly extended red tail appears in the scattered radiation. We also find that the linear degree of polarization of singly Thomson scattered line radiation is wavelength-dependent and that there are significant differences in the linear degree of polarization from that computed from classical physics in the far red tail. We propose that the semi-forbidden broad emission line C III]1909 may be significantly contributed from Thomson scattering because this line has small resonance scattering optical depth in the broad absorption line region, which leads to distinct and significant polarized flux in this broad emission line.

Key words : polarization — radiative transfer — scattering — galaxies:nuclei — quasars

I. INTRODUCTION

Active galactic nuclei (hereafter AGN) are believed to be powered through graviational attraction of material by a supermassive black hole with mass up to 10^9 $M_\odot$. Quasars are the most luminous objects classified as AGN. The typical mass accretion rate amounts to $\dot{M} \sim 1$ $M_\odot$ yr^{-1}, yielding a luminosity $L \sim 10^{45}$ erg s^{-1}. Most quasar spectra are characterized by nonthermal continuum and prominent broad emission lines with a width $\Delta v \sim 10^4$ km s^{-1} that are believed to be Doppler broadened (e.g. Krolik 1999). Investigations using the reverberation mapping show that the broad emission line region may reside within one parsec of the quasar central engine (Peterson 1993).

About 10 percent of quasars are known to exhibit deep broad absorption troughs blueward of prominent permitted emission lines. These quasars showing P-Cygni type profiles in their permitted lines are called broad absorption line quasars (BALQ's hereafter). According to the studies of Turnshek (1984) the equivalent widths of the emission part are statistically similar to those of normal quasars. This strongly implies that BALQ's are normal quasars viewed from special directions and that the broad absorption line region typically covers 10 percent of the quasar central emission region.

Arav (1996) noted the existence of ghost features in the absorption troughs of C IV 1550 that are formed at the velocity $v = -5900$ km s^{-1}. He attributed the ghost features to the abrupt decrease of the optical depth at this velocity by the sudden increase of radiative acceleration by Lyα photons that are resonantly scattered with the transition $2S_{1/2} - 2P_{1/2,3/2}$ by N V ions (Arav et al. 1995). The presence of these ghost features implies that the material responsible for the broad absorption troughs is radiatively accelerated just outside the broad emission line region in quasars.

The origin of these deep absorption troughs is still controversial. One plausible suggestion is that they are usually attributed to the existence of outflows slightly above the accretion disk around the supermassive black hole (Murray & Chiang 1995). In this accretion disk wind scenario, the coronal material above the accretion disk may be accelerated by the strong quasar radiation up to velocities of $0.2c$, where c is the speed of light.

According to this unification view of BALQ's with the accretion disk wind, it is naturally expected that

Corresponding Author: H.-W. Lee

some fraction of line photons scattered from other directions may enter the observer's line of sight. Because scattered radiation is usually polarized, spectropolarimetry can be a useful tool to investigate the unification model of BALQ's.

Spectropolarimetry is an important study of unification of broad line AGN and narrow line AGN since broad Hβ emission profile was found in the polarized spectrum in the prototypical Seyfert 2 galaxy NGC 1068 (Antonucci & Miller 1985, Antonucci et al. 1996). A similar study was done for the narrow line radio galaxy Cyg A by Ogle et al. (1997), who found a very broad polarized feature around Hα.

Lee & Blandford (1997) considered both jet and disk wind model for BAL outflows to compute the linear polarization of resonance doublets and singlets. They adopted a Monte Carlo technique incorporating the Sobolev approximation, because the velocity scale associated with the BAL flows is much larger than the thermal velocity scale. They showed that high degree of linear polarization is expected in the broad absorption troughs for an accretion wind disk model.

Wang, Wang & Wang (2005) considered polarized radiative transfer in BALQ's and they tentatively concluded that the polarimetric behavior of BALQ's is better explained when they include electron scattering in addition to resonance scattering. According to the photoionization computations by Murray & Chiang (1998), the total column density of the BAL region will not greatly exceed 10^{24} cm^{-2}, in which case the BAL region is Thomson optically thin.

Cohen et al. (1995) presented their spectropolarimetric observations of the BALQ PHL 5200, in which the high degree of polarization appeared in the blue troughs of permitted lines including C IV 1550, lending strong support to the accretion disk wind model. A similar conclusion has been reached by a more extensive spectropolarimetric studies of BALQ's carried out by Ogle et al. (1999).

Thus far, no relativistic effects have been considered in previous investigations of polarized radiation in BAL flows. In view of the fact that the outflow velocity scale is up to $0.2c$, the relativistic aberration effect may not be negligible, and hence polarization will be severely affected in the scattered radiation. We want to address this issue in this work by investigating the Thomson scattered flux and linear polarization of singly scattered radiation.

In the next section, we describe Thomson scattering with the special relativistic effects, and the Monte Carlo code to compute the linear polarization. In Section 3, we present our calculation of polarized Thomson scattered lines in an accretion disk wind that may be appropriate for a typical BALQ. In the final section, we briefly discuss our results.

II. MONTE CARLO PROCEDURE

In this section, we describe briefly the computation procedure for the polarized line emission in quasars. In this work, we approximate the broad absorption line region by a disk-like distribution moving radially outward. For simplicity, we only consider an azimuthally symmetric distribution, where the outflow velocity is purely radial.

In Fig. 1, we show a schematic diagram for the scattering geometry considered in this work. Line photons are assumed to be generated in the close vicinity of the center where the supermassive black hole of the quasar is located. The incident line photons catch up with the scattering cloud moving along the same direction to be subsequently scattered and enter the observer's line of sight.

First, we consider a ring-like distribution of outflowing gas cloud with a specific velocity $v = c\beta$. We prepare photons generated near the center that are incident on an outflowing single cloud. For a single scattering of a line photon with the incident wavevector $\hat{\mathbf{k}}_i = (\sin\phi_i, \cos\phi_i, 0)$ and the outgoing wavevector $\hat{\mathbf{k}}_o = (\cos\theta_o \cos\phi_o, \cos\theta_o \sin\phi_o, \cos\theta_o)$, the linear degree of polarization is given by

$$p = \frac{1-\mu^2}{1+\mu^2}, \tag{1}$$

where the two unit vectors make an angle $\theta = \cos^{-1}\mu$ given by

$$\mu = \hat{\mathbf{k}}_i \cdot \hat{\mathbf{k}}_o. \tag{2}$$

(e.g. Rybicki & Lightman 1979).

However, when β is not negligible, the special relativistic effect should be considered with full care. In our Monte Carlo code, we consider the scattering process in the rest frame of the scatterer, where the outgoing wavevector is chosen with the dipole distribution

$$f(\mu) = 1 + \mu^2. \tag{3}$$

Once the outgoing wavevector is chosen in the rest frame of the scatterer, it is transformed to the observer's rest frame using the Lorentz transformation

$$\mu' = \frac{\mu + \beta}{1 + \beta\mu}, \tag{4}$$

which is well-known as the aberration effect of light.

Then the degree of polarization $p(\mu)$ computed in the rest frame of the scatterer as in Eq. (1) is translated into

$$p_{obs}(\mu') = p(\mu). \tag{5}$$

In our Monte Carlo code, the polarization state of a given line photon is described by a density matrix ρ, which is computed in the rest frame of the scatterer (e.g. Lee, Blandford & Western 1994, Lee 1999).

It is necessary to obtain the expression for the outgoing wavevector $\hat{\mathbf{k}}_o^{obs}$ in the observer's rest frame when we have $\hat{\mathbf{k}}_o$ in the rest frame of the scatterer that makes an angle θ given by Eq. (2). Because $\hat{\mathbf{k}}_o^{obs}$ is in the plane spanned by $\hat{\mathbf{k}}_i$ and $\hat{\mathbf{k}}_o$, we have

$$\hat{\mathbf{k}}_o^{obs} = a\hat{\mathbf{k}}_i + b\hat{\mathbf{k}}_o. \tag{6}$$

Using the fact that the unit vectors $\hat{\mathbf{k}}_o^{obs}$ and $\hat{\mathbf{k}}_i$ make an angle $\theta' = \cos^{-1}\mu'$ satisfying Eq. (4), we may obtain in a straightforward way the coefficients a and b as

$$\begin{aligned} a &= \cos(\theta' - \theta)/\sin\theta \\ b &= \sin\theta'/\sin\theta. \end{aligned} \tag{7}$$

We denote the frequency of the incident radiation by ν_i. In the rest frame of the single cloud that is moving outward with speed $v = c\beta$, the photon frequency becomes $\nu_{i,scat} = \nu_i[(1-\beta)/(1+\beta)]^{1/2}$, because the incident photon is moving right toward the cloud. In the rest frame of the scatterer, this frequency is also that of the outgoing photon because of the energy conservation. In this work, we assume that the photon energy is much less than the electron rest mass energy. Therefore, the frequency of the outgoing photon in the observer's rest frame is obtained by the Lorentz transformation to be

$$\nu_o = \nu_{i,scat}/[\gamma(1-\beta\mu')] = \frac{1-\beta}{1-\beta\mu'}\nu_i, \tag{8}$$

where $\gamma = (1-\beta^2)^{-1/2}$ is the Lorentz factor of the moving cloud. In our Monte Carlo calculation, we are interested in the frequency shift relative to the line center for a given atomic transition. The relative frequency shift $\Delta x = \Delta\nu/\nu_i = (\nu_o - \nu_i)/\nu_i$ per scattering measured in the observer's rest frame is given by

$$\Delta x = \frac{\beta(\mu'-1)}{1-\beta\mu'}, \tag{9}$$

which is compared with the non-relativistic expression Δx_{nr} given by

$$\Delta x_{nr} = \beta(\mu - 1). \tag{10}$$

As is clearly seen, no frequency shift is observed in the case of forward scattering (i.e. $\mu' = \mu = 1$) for both relativistic and non-relativistic situations. It should be noted that the difference of Δx and Δx_{nr} is given as an order of β^2. The biggest difference for the frequency shift is obtained for backward scattering, in which case we have $\Delta x = -2\beta/(1+\beta)$ and $\Delta x_{nr} = -2\beta$.

Based on the numerical result of the single cloud case, we consider a ring-like distribution of single clouds that are radially moving outwards with speed $v = c\beta$. In our Monte Carlo code, we collect scattered photons according to their wavelength and the $z-$component of their unit wavevector.

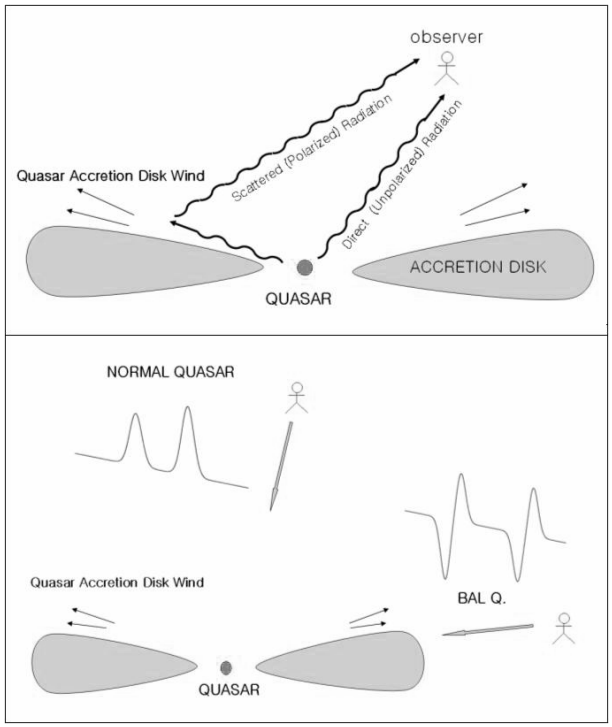

Fig. 1.— A schematic diagram showing our scattering geometry for a quasar with a broad absorption line region. The scattering material is distributed around the quasar engine forming a set of rings that are moving outward with velocity $v = c\beta$, where β has a range $0 < \beta < 0.2$. In this work, we only consider the flux and linear polarization of singly scattered radiation.

Finally, we consider the Thomson optically thin broad absorption line region as a collection of these rings consisting of single clouds with a range $\beta \leq 0.2$. In our Monte Carlo code, we choose a scattering cloud located in the equatorial plane and assign it a speed β by multiplying 0.2 with a uniform random number r generated in the unit interval $(0, 1)$ to simulate the disk-like electron scattering region.

III. RESULTS

(a) Polarization of Radiation Scattered from a Single Cloud

In Fig. 2, we show the polarization of singly Thomson scattered radiation from a set of moving single clouds with speed $\beta = 0, 0.1, 0.2$ and 0.7. Here, we assume that the emission source is monochromatic in order to concentrate on the variation of the flux distribution and linear degree of polarization as a function of the observer's line of sight with respect to the direction of the cloud motion. The case $\beta = 0.7$ is unrealistically high for our application to the scattering region of a typical broad absorption line quasars. However, we include this case, because with an extreme β it is easy to

recognize the relativistic effects. We also include the case $\beta = 0$ in order to obtain the polarization that is purely classical, to which our relativistic computation should be reduced in the limit $\beta \to 0$.

In this case of $\beta = 0$, the incident photons are prepared to propagate along $z-$axis, where a moving cloud with speed $v = c\beta$ is located. In each panel, we show the scattered flux by a solid line as a function of the cosine of the angle $\theta_o = \cos^{-1}\mu_o$ between the $z-$axis and the observer's line of sight. The linear degree of polarization is also represented by crosses.

When $\beta = 0$ the flux distribution conforms the dipolar one given by Eq. (3), where we expect twice more photons in both forward and backward direction $\mu = \pm 1$ than in the direction $\mu = 0$ perpendicular to $z-$axis. The flux distribution and the linear degree of polarization are both symmetric with respect to $\mu = 0$, where the maximum degree of polarization $p_{deg} = 1$ is shown.

However, this symmetric flux distribution is no longer seen in other cases with $\beta > 0$. Because of the relativistic beaming effect, the symmetric dipolar flux distribution in the rest frame of the single cloud becomes asymmetric toward positive μ. It is also interesting that the flux distribution is a monotonically increasing function of μ in the case of $\beta = 0.7$, where the flow velocity is unrealistically high. In particular, the maximum degree of polarization is seen near $\mu = \beta$, which is naturally expected because $\mu = 0$ is transformed into $\mu' = \beta$ according to Eq. (4). The asymmetry of the flux distribution and linear degree of polarization is attributed to the special relativistic aberration effect summarized by Eq. (4).

(b) Polarization from a Ring-like Distribution of Single Clouds

In this subsection, we consider a collection of single clouds that are distributed in the shape of a ring moving outwards with speed $v = c\beta$. The emission source is assumed to be located at the center of the ring and has a Gaussian profile given by

$$\phi_\nu = \phi_0 \exp[-0.035\Delta x^2], \tag{11}$$

for which the full width at half maximum corresponds to 2.5×10^4 km s^{-1}. The positive value of Δx corresponds to the blue part with respect to the line center.

Fig. 3 shows the flux distribution and the linear degree of polarization for $\beta = 0, 0.1$ and 0.2. In the left panel, we show the numerical data for those line photons scattered with $\mu_o = \cos\theta_o = -0.8 \pm 0.05$, where θ_o is the angle between the normal direction to the ring and the observer's line of sight. The right panel shows the our numerical data for $\mu_o = -0.4$. Here, the sign of the degree of polarization represents the position angle of the polarization, where the negative degree of polarization shows polarization parallel to the axis that is normal to the ring and the positive degree is for perpendicular polarization.

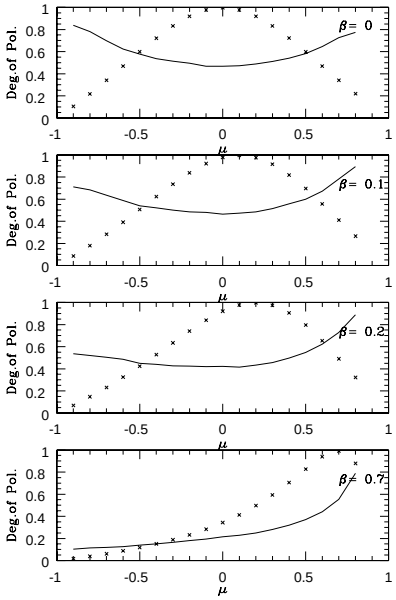

Fig. 2.— Linear degree of polarization and flux of the line radiation scattered from a single cloud that is moving with speed $v = c\beta$. The horizontal axis represents the cosine of the angle between the direction of the cloud motion and the observer's line of sight. The vertical axis shows the linear degree of polarization.

For $\beta = 0$, corresponding to stationary clouds, no frequency shift is observed, so that the flux distribution shows the exactly the Gaussian profile of the emission source given in Eq. (11). Furthermore, the linear degree of polarization is constant because the cosine of the angle between the incident and scattered radiation is constant with no frequency shift.

However, for $\beta = 0.1$ and 0.2, the flux profile and the linear degree of polarization show very rich and complicated structures. The center of the flux profile tends to move redward as β increases, which is attributed to the relativistic Doppler effect. The flux profile is asymmetric with respect to the overall line center. In particular, the profiles exhibit double-peak structures that are also asymmetric with the stronger blue peak. This double-peak structure is expected from the dipolar distribution of Thomson scattering given by Eq. (3), which produce more forward (with no frequency shift) and backward (with maximum redward frequency shift) radiation out of a single Gaussian emission line. The blueward asymmetry in the line profile reflects the tendency of yielding more photons in the forward direction than in the backward direction, which is the aspect of the relativistic aberration.

The degree of polarization shows maximum near the center of the flux profile, where it is contributed significantly from scattered component at right angle. It is particularly interesting that the polarization flip occurs conspicuously in the far blue wing regions and some-

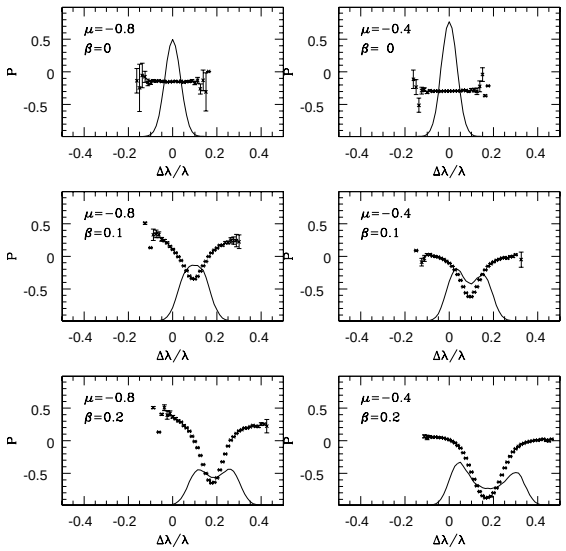

Fig. 3.— Linear degree of polarization and flux of the line radiation scattered from a ring of single clouds that are moving with speed $v = c\beta$ with $\beta = 0, 0.1$ and 0.2. The horizontal axis shows the fractional frequency shift $\Delta x = \Delta\nu/\nu_i$ and the vertical axis shows the linear degree of polarization. The negative degree of polarization means the polarization direction parallel to the direction that is normal to the ring, and positive degree for perpendicular direction. In the left panel, the observer's line of sight makes an angle θ with the ring normal with $\mu = \cos\theta = -0.8$ and the right panel is for $\mu = -0.4$.

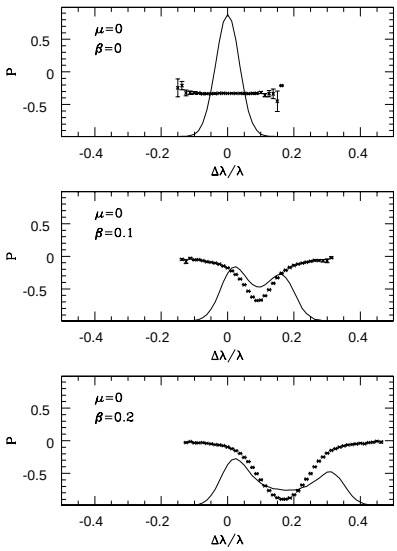

Fig. 4.— The same as Fig. 3 except for the observer's line of sight is $\mu = 0$, for which case the observer is in the equatorial plane.

what less in the far red wings. The polarization structures and the flux profiles are closely related and coupled, because both the frequency shift and the degree of polarization is determined by the angle between the directions of incident and scattered radiation that is also affected from the kinematics of the clouds.

Fig. 4 shows the same numerical data that is observed to the observer in the equatorial direction $\mu_o = 0 \pm 0.05$. Qualitatively, a similar result is obtained to those for the observers at $\mu_o = -0.8$ and $\mu_o = -0.4$. In the case of $\beta = 0$, the linear degree of polarization is 1/3, as is expected for a dipole radiation.

(c) Polarization from an Optically Thin Broad Absorption Line Region

In this subsection, we consider a disk-like distribution of scattering clouds, which is approximated as a collection of rings that are moving outwards with speed $v = c\beta$ with $0 < \beta < 0.2$. In Fig. 5 we show the flux and the linear degree of polarization of singly Thomson scattered line radiation according to the line of sights with $\mu_o = -0.8, -0.4$ and 0. In the left panel, the maximum speed of the broad absorption line region is $\beta = 0.2$, whereas in the right panel we consider the annular region of moving clouds with maximum speed $\beta = 0.1$. In the left panel, the flux profiles are more asymmetric than the counterparts shown in the right panel.

It is particularly notable that the linear degree of polarization in the singly scattered radiation is wavelength-dependent. The largest degree of polarization $\simeq 0.5$ occurs at $\Delta\lambda/\lambda \simeq 0.1$ for $\mu = 0$. Similar behaviors with weaker polarization are seen for $\mu = -0.4$ and $\mu = -0.8$. It is also notable that there is polarization flip in the far red wing for $\mu = -0.8$.

In Fig. 6 we compare our result in Fig. 5 for $\mu = -0.4$ and $\beta = 0.2$ with that obtained for the same condition without considering the special relativistic effect. The flux profile obtained using classical physics is shown by a dotted line, whereas the solid line shows the result in Fig. 5 for $\mu = -0.4$. The crosses represent the linear degree of polarization calculated in the frame of special relativity shown in Fig. 5, and the filled triangles show the result of classical calculation.

As is expected, the deviation is seen in the far red wing, where the relativistic effect is the largest. As we discussed in the previous section, the red wing is less extended when we consider the special relativity. In particular, the linear degree of polarization at $\Delta\lambda/\lambda = 0.2$ is 0.24 in the case of classical calculation, whereas it is 0.17 when we take the special relativistic effect into consideration. This large difference is due to the coupling of the scattering angle and frequency shift by the relativistic Doppler and aberration effects.

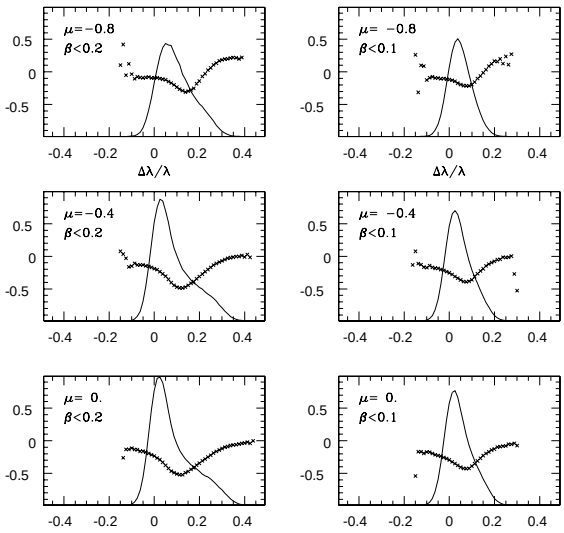

Fig. 5.— The flux and the linear degree of polarization of singly scattered radiation from a disk-like distribution of clouds moving radially outward. In the left panel, the speed distribution of the clouds is $\beta < 0.2$ and in the right panel it is $\beta < 0.1$. We see much extended red tails and more asymmetric profiles.in the case $\beta < 0.2$.

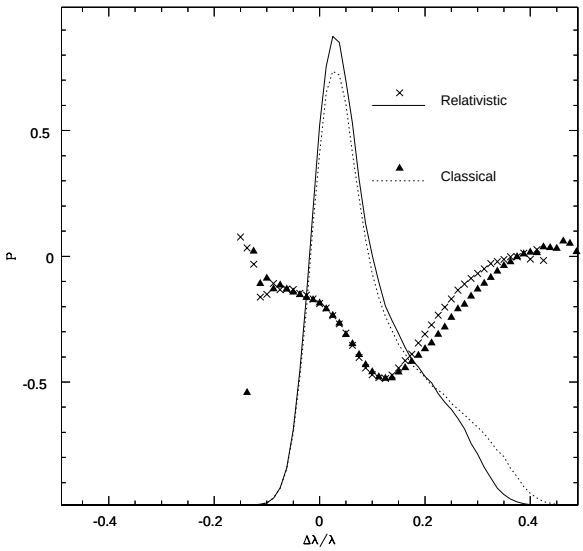

Fig. 6.— A comparison of results obtained from classical physics and from full consideration of special relativity for the flux profile and the linear degree of polarization. The flux profile for classical physics is shown by a dotted line, whereas the solid line shows the result in Fig. 5 for $\mu = -0.4$. The crosses represent the linear degree of polarization calculated in the frame of special relativity shown in Fig. 5, and the filled triangles show the result of classical calculation.

IV. SUMMARY AND DISCUSSION

In this work, we compute the flux and the linear degree of polarization of the line radiation that is singly Thomson scattered in a disk-like region moving outwards with speed $v = c\beta < 0.2c$, taking a full consideration of special relativistic effects. When the velocity of the broad absorption region is limited to $\beta < 0.2$, the frequency shift exhibited in the scattered radiation may extend to $\Delta x \simeq 0.4$ forming an extended red tail that is significantly polarized. Interplay between the kinematics and the special relativistic aberration effect results in rich and complicated structures in linear polarization.

However, the singly Thomson scattered line radiation will be mixed with the unpolarized direct continuum, which will reduce the linear degree of polarization significantly. Furthermore, prominent emission lines observed in quasars are usually resonance doublets, arising from transitions $S_{1/2} - P_{1/2,3/2}$. These include Lyman series of hydrogen, O VI 1034, N V 1240, and C IV 1550 to name a few. In particular, it is well-known that much weaker polarization is expected for these doublets than that for singlet transitions (e.g. Lee et al. 1994, Stenflo 1980). The polarization for resonantly scattered radiation is deferred to the future work.

Cohen et al. (1995) noted that the broad semi-forbidden line C III]1909 is significantly polarized in the quasar PHL 5200. Lee et al. (1994) proposed that this semi-forbidden line can be polarized from anisotropic clouds in the broad emission line region. However, since this intercombination line is expected to have small resonance scattering optical depth in the broad absorption line region, we may consider that this broad emission line may be significantly contributed from the Thomson scattered radiation. This will lead to distinctly strong polarized flux in this emission line compared to other permitted broad emission lines. More spectropolarimetric observation and future investigations of resonantly scattered radiation may shed more light on this point.

ACKNOWLEDGEMENTS

The authors gratefully acknowledge financial support from the Korea Science and Engineering Foundation (KOSEF) through the Research and Education Program for Science High Schools (R&E Program).

REFERENCES

Antonucci, R., Geller, R., Goodrich, R. W., & Miller, J. S., 1996, The Spectropolarimetric Test of the Quasar Emission Mechanism, ApJ, 472, 502

Antonucci, R. & Miller, J. S., 1985, Spectropolarimetry and the Nature of NGC 1068, ApJ, 297, 621

Arav, N., 1996, The "Ghost of Ly alpha" as Evidence for Radiative Acceleration in Quasars, ApJ, 465, 617

Arav, N., Korista, K. T., Barlow, T. A., & Begelman, M. C., 1995, Radiative Acceleration of Gas in Quasars, Nature, 376, 576

Cohen, M. H., Ogle, O. M., Tran, H. D., Vermeulen, R. C., Miller, J. S., Goodrich, R. W., & Martel, A. R., 1995, Spectropolarimetry of Two Broad Absorption Line Quasars with the W. M. Keck Telescope, ApJ, 448, 77

Krolik, J. H., 1999, Active Galactic Nuclei : from the Central Black Hole to the Galactic Environment, Princeton University Press, Princeton

Lee, H. -W., 1999, Polarization Structures in the Thomson-scattered Emission in Active Galactic Nuclei, ApJ, 511, L13

Lee, H. -W. & Blandford, R. D., 1997, On the Polarization of Resonantly Scattered Emission Lines III- Polarization of Quasar Broad Emission Lines and Broad Absorption Line Troughs, MNRAS, 288, 19

Lee, H. -W., Blandford, R. D., & Western, L., 1994, On the Polarization of Resonantly Scattered Emission Lines I- Emission and Absorption Coefficients in an Anisotropic Radiation Field, MNRAS, 267, 303

Murray, N. & Chiang, J., 1995, Active Galactic Nuclei Disk Winds, Absorption Lines and Warm Absorbers, ApJ, 454, L105

Murray, N. & Chiang, J., 1998, Photoionization of Nuclei Disk Winds, ApJ, 494, 125

Ogle, P. M., Cohen, M. H., Miller, J. S., Tran, H. D., Fosbury, R. A. E., & Goodrich, R. W., 1997, Scattered Nuclear Continuum and Broad H alpha in Cygnus A, ApJ, 482, L37

Ogle, P. M., Cohen, M. H., Miller, J. S., Tran, H. D., Goodrich, R. W., & Martel, A. R., 1999, Polarization of Broad Absorption Line QSOs. I. Spectropolarimetric Atlas, ApJS, 125, 1

Peterson, B. M., 1993, Reverberation Mapping of Active Galactic Nuclei, PASP, 105, 247

Rybicki, G. B. & Lightman, A. P., 1979, Radiative Processes in Astrophysics, A Wiley-Interscience Publication, New York

Stenflo, J. O., 1980, Resonance Line Polarization. V. - Quantum Mechanical Interference between States of Different Total Angular Momentum, A&A, 84, 68

Turnshek, D. A., 1984, Properties of the Broad Absorption Line QSOs, ApJ, 280, 51

Wang, H. -Y., Wang, T. -G., & Wang, J. -X., 2005, Polarization of Quasars; Electron Scattering in the Broad Absorption Line Region, ApJ, 634, 149